

Molecular Gas and the Modest Star Formation Efficiency in the “Antennae” Galaxies: Arp 244=NGC 4038/9

Yu Gao^{1,2,3}, K.Y. Lo^{3,4}, S.-W. Lee^{2,4}, & T.-H. Lee^{4,5}

gao@ipac.caltech.edu, kyl@asiaa.sinica.edu.tw, swlee@fft.astro.utoronto.ca,
thlee@iras.ualgary.ca

ABSTRACT

We report here a factor of 5.7 higher total CO flux in Arp 244 (the “Antennae” galaxies) than that previously accepted in the literature (thus a total molecular gas mass of $1.5 \times 10^{10} M_{\odot}$), based on our fully sampled CO(1-0) observations at the NRAO 12m telescope. Currently, much of the understanding and modeling of the star formation in Arp 244 has been derived from a much lower molecular gas mass. It is imperative to reconsider all as the high molecular gas mass might provide sufficient fuel for ultraluminous extreme starburst in Arp 244 once the merging advances to late stage.

Our observations show that the molecular gas peaks predominately in the disk-disk overlap region between the nuclei, similar to the far-infrared (FIR) and mid-infrared (MIR) emission. The bulk of the molecular gas is forming into stars with a normal star formation efficiency (SFE) $L_{\text{IR}}/M(\text{H}_2) \approx 4.2 L_{\odot}/M_{\odot}$, same as that of giant molecular clouds in the Galactic disk. Additional supportive evidence is the extremely low fraction of the dense molecular gas in Arp 244, revealed by our detections of the HCN(1-0) emission, which traces the active star-forming gas at density $\gtrsim 10^4 \text{ cm}^{-3}$.

Using the high-resolution BIMA plus the NRAO 12m telescope, full-synthesis CO(1-0) images, and our VLA continuum maps at 20cm, we estimate the local SFE indicated by the ratio map of the radio continuum to CO(1-0) emission, down to kpc scale. Remarkably, the local SFE stays roughly same over the bulk of the molecular gas distribution. Only some localized regions show the highest radio-to-CO ratios that we have identified as the sites of the most intense starbursts with $\text{SFE} \gtrsim 20 L_{\odot}/M_{\odot}$. Here we have assumed that the 20cm emission is a fairly good indicator of star formation down to kpc scale in Arp 244 because of the well-known correlation between the FIR and the radio continuum emission. These starburst regions are confined exclusively in the dusty patches seen in the HST optical images near the CO and FIR peaks where presumably the violent starbursts are heavily obscured. Nevertheless, recent large-scale star formation is going on throughout the system (e.g., concentrations of numerous super-star clusters and MIR “hotspots”), yet the measured level is more suggestive of a moderate starburst ($\text{SFE} \gtrsim 10 L_{\odot}/M_{\odot}$) or a weak to normal star formation ($\text{SFE} \sim 4 L_{\odot}/M_{\odot}$), not necessarily occurring at the high concentrations of the molecular gas reservoir. The overall starburst from the bulk of the molecular gas is yet to be initiated as most of the gas further condenses into kpc scale in the final coalescence.

Subject headings: galaxies: individual (NGC 4038/9) — galaxies: interactions — galaxies: starburst — infrared: galaxies — ISM: molecules — stars: formation

¹Infrared Processing and Analysis Center, Jet Propulsion Laboratory, Caltech 100-22, 770 S. Wilson Ave., Pasadena, CA 91125

²Department of Astronomy, University of Toronto, 60

St. George Street, Toronto, ON M5S 3H8, CANADA

³Laboratory for Astronomical Imaging, Department of Astronomy, University of Illinois, 1002 W. Green Street, Urbana, IL 61801

⁴Institute of Astronomy and Astrophysics, Academia

1. INTRODUCTION

The “Antennae” galaxies (Arp 244, NGC 4038/39, VV 245), the nearest IR-luminous and perhaps the youngest prototypical galaxy-galaxy merger (the first in Toomre (1977) merger sequence), certainly reclaimed its fame from the recent releases of the HST/WFPC2 images (Whitmore et al. 1999) and the Chandra X-ray images (Fabbiano et al. 2000), and the observations at essentially all available wavelengths from radio to X-ray (e.g., Hummel & van der Hulst 1986; Neff, & Ulvestad 2000; Hibbard, van der Hulst, & Barnes 2001 in preparation; Bushouse, Telesco, & Werner 1998; Nikola et al. 1998; Mirabel et al. 1998; Vigroux et al. 1996; Read, Ponman, & Wolstencroft 1995; Fabbiano, Schweizer, & Mackie 1997). The HST images reveal over one thousand bright young star clusters that are thought to have formed in recent bursts of star formation. H α imaging also shows the most recent locations of the star-forming giant HII regions and their velocity fields as well (Rubin, Ford, & D’Odorico 1970; Amram et al. 1992; Whitmore et al. 1999). Soft X-ray (Fabbiano et al. 1997) and radio continuum (Hummel & van der Hulst 1986) images may hint of previous star formation sites currently seen as supernova remnants. In addition, mid-infrared (MIR) (Mirabel et al. 1998; Vigroux et al. 1996), far-infrared (FIR) (Evans, Harper, & Helou 1997; R. Evans 1998, private communications; Bushouse et al. 1998) and sub-millimeter (Haas et al. 2000) images indicate that the most intense starburst takes place currently in an off-nucleus region that is inconspicuous at optical wavelengths. The star-forming molecular gas in Arp 244 is perhaps least understood, however; we show in this paper that the total molecular gas mass accepted in the literature for the last decade (Sanders & Mirabel 1985; Stanford et al. 1990) has been underestimated by nearly a factor of 6.

The importance of gas during galaxy-galaxy merging far exceeds its mass proportion, as demonstrated by the sophisticated numerical simulations (e.g., Barnes & Hernquist 1996, 1998). At a distance of 20 Mpc ($H_0 = 75\text{km s}^{-1} \text{Mpc}^{-1}$,

e.g., van der Hulst 1979; Mihos, Bothun, & Richstone 1993; Mirabel et al. 1998), the total IR luminosity (8–1000 μm , Sanders & Mirabel 1996) of Arp 244, measured from the *IRAS* four-band fluxes given in Soifer et al. (1989), is $L_{\text{IR}} = 6.2 \times 10^{10} L_{\odot}$. Using the most recent remeasured total *IRAS* fluxes (as opposed to simply the “point source” in Soifer et al. 1989) in the Revised Bright Galaxy Sample (D.B. Sanders 2000, private communication; Sanders, Mazzarella, Kim, & Surace 2001 in preparation), the same IR luminosity is obtained. Therefore, strictly speaking Arp 244 is not a luminous infrared galaxy (LIG, $L_{\text{IR}} \gtrsim 10^{11} L_{\odot}$) unless a Virgocentric flow distance of 29.5 Mpc is used (Sanders et al. 2000, but we use 20 Mpc throughout this paper), which leads to $L_{\text{FIR}} = 1.0 \times 10^{11} L_{\odot}$ and $L_{\text{IR}} = 1.3 \times 10^{11} L_{\odot}$. A much smaller molecular gas mass of $2.6 \times 10^9 M_{\odot}$ (Sanders & Mirabel 1985), currently accepted in the literature, leads to a higher global ratio of $L_{\text{IR}}/M(\text{H}_2) \sim 24 L_{\odot}/M_{\odot}$. This ratio is often referred as the star formation efficiency (SFE) since the FIR emission, tracer of current star formation rate, has been normalized by the molecular gas mass available to make stars. With this high yield of young stars per unit molecular gas mass and a lower molecular gas content, most of the molecular gas will be depleted in $\sim 10^8$ years, as noted by Sanders & Mirabel (1985) and Stanford et al. (1990). There would be no chance for Arp 244 to become an ultraluminous infrared galaxy (ULIG, $L_{\text{IR}} \gtrsim 10^{12} L_{\odot}$) in the late stage of the merging. Numerical modeling (Mihos et al. 1993), based on this lower gas mass, indeed predicted that Arp 244 would not join the rank of ULIGs.

ULIGs, with the IR luminosity comparable to the bolometric luminosity of QSOs, are the most luminous galaxies in the local universe. They are believed to be powered mainly by starbursts (e.g., Smith, Lonsdale, & Lonsdale 1998; Genzel et al. 1998) taking place predominantly in the *extreme starburst* regions of a characteristic size of ~ 100 pc and $L_{\text{IR}} \sim 3 \times 10^{11} L_{\odot}$ (Downes & Solomon 1998), produced as a result of the merging of molecular *gas-rich* spiral galaxies (Sanders & Mirabel 1996). Alternatively, the dust-enshrouded active galactic nuclei (AGN) may still be responsible for significant energy output in some ULIGs (Sanders et al. 1988; Veilleux,

Sinica, P.O. Box 1-87, Nankang, Taipei, Taiwan

⁵Department of Physics and Astronomy, University of Calgary, 2500 University Drive, N.W., Calgary, Alberta T2N 1N4, CANADA

Sanders, & Kim 1999; Sanders 1999). Now, for a total molecular gas mass of $1.5 \times 10^{10} M_{\odot}$, based on our fully sampled CO(1-0) observations obtained at the NRAO ⁶ 12m, many previous conclusions and speculations about Arp 244 need to be revised. After all, the initial gas content, particularly the molecular gas — the fuel for star formation, will probably be the most important factor in determining whether a merging pair of spiral galaxies reaches the peak of ultraluminous extreme starburst phase since all ULIGs are still gas-rich with $\sim 10^{10} M_{\odot}$ molecular gas mass (Solomon et al. 1997), most likely concentrated in the kpc scale disks/rings around the merging nuclei (Downes & Solomon 1998; Scoville, Yun, & Bryant 1997; Sakamoto et al. 1999; cf. Evans, Surace, & Mazzarella 2000).

With a molecular gas mass comparable to that of ULIGs and an early/intermediate merging stage, Arp 244 is perhaps an example of what an ULIG might have looked like a few hundred million years ago. Arp 244 may be a snapshot in the evolution of a typical gas-rich merger into an ULIG system. Thus, it is crucial to understand how, where and when the starbursts initiate or have occurred in such an on-going merger. This becomes especially imperative in Arp 244 given the advantage of its close-up distance and therefore the better linear resolution available. Nonetheless, the strongest starburst site revealed from the Infrared Space Observatory (*ISO*) MIR images (Vigroux et al. 1996; Mirabel et al. 1998; Xu et al. 2000) seems to be offset from the peak emission in all the 60, 100, and 160 μm FIR maps of the limited resolution, obtained with the Kuiper Airborne Observatory (KAO, Evans, Harper, & Helou 1997; Bushouse et al. 1998). In order to best locate the sites of the intense star formation, high-resolution imaging in the FIR is ultimately required.

Since there is an excellent correlation between the FIR and the radio continuum emission (e.g., Helou, Soifer, & Rowan-Robinson 1985; Condon et al. 1990; Condon 1992; Xu et al. 1994; Marsh & Helou 1995), the FIR emission can thus be approximately scaled according to the radio contin-

uum emission with the high resolution achievable by the Very Large Array (VLA) observations. We have therefore, obtained the VLA radio continuum images to compare with our high-resolution full-synthesis Berkeley-Illinois-Maryland Association (BIMA) plus the NRAO 12m CO maps. This is because the star formation occurs within giant molecular clouds (GMCs), especially the dense cores and starburst can be better characterized by the elevated SFE, i.e., the FIR to CO ratio, approximated here by the radio-to-CO ratio. Therefore, local SFE across over the merging system can be approximately measured using the ratio map of the radio continuum to the CO emission to locate the most intense starburst sites of the highest radio-to-CO ratios.

We here briefly report our various observations in §2 detailing the single-dish CO mapping in Arp 244. The BIMA interferometry CO and the VLA 20cm continuum observations will be presented elsewhere. The observational results and analysis are summarized and compared in §3. Section 4 discusses the starburst properties of Arp 244 and the implications of our observations. Finally, we conclude our main results.

2. OBSERVATIONS

We obtained the NRAO 12m single-dish CO(1-0) map at Nyquist sampling (half-beam spacing $\sim 27.''5$) in order to determine the true total CO extent and distribution and help add in the zero-spacing flux missed from the multifield BIMA CO(1-0) data cube. A total of more than 50 positions have been observed in 1998 March and 20 more positions in the outer edge of the map were further obtained in 1998 April to fully cover the entire CO emission region. We have essentially integrated for at least 1.5 hr at every position in order to make sure that not only no further $\gtrsim 3\sigma$ level CO emission is detected in the outmost edge of the map but all spectra obtained at different positions have roughly comparable RMS noise level as well. A total of 73 positions have been mapped in the merging disks accumulating more than 110 hr useful integration time. Additional observations in 1999 June and November have been conducted remotely in the southeastern (SE) extension of the disk overlap region (where the much longer southern tidal tail starts) and at the tip of the southern

⁶The National Radio Astronomy Observatory is a facility of the National Science Foundation operated under cooperative agreement by Associated Universities, Inc.

tail (Figure 1). This is to further integrate down the noise level to clearly show that CO is detected significantly far away from the merging disks, and to possibly search for CO emission at the location of the tidal dwarf galaxy, several tens of kpc away from the merging disks. The typical integration time at each of these selected positions is more than 3 hr. We have tried several positions at the tip of the southern tidal tail and deep integrations in the possibly detected positions were further conducted in 2000 March and April, totaling 27 hr usable integration time in this tidal feature area.

We used the dual SIS 3mmhi receivers connected with both the two 256×2 MHz filter banks and the two 600 MHz spectrometers providing a velocity resolution of 2MHz \sim 5 km s⁻¹ and a total velocity coverage of 1330 km s⁻¹. The system temperature T_{sys} (SSB) was typically less than 400 K (on a T_R^* scale) and the weather conditions were excellent throughout almost all observing runs. Occasionally, exceptional weather with $T_{\text{sys}} \sim$ 200 K (for a low-decl. southern sky source at 115 GHz!) was seen in a few days. All observations were performed using a subreflector nutating at a chop rate of 1.25 Hz with a beam throw of $\pm 3'$ plus a position switch (the so-called “BSP” mode) to achieve the flat baselines. This ensures that the off-source reference sky position is 6' away from the observed on-source pointing so that the telescope beam (FWHM \sim 55") at the reference position is well outside the CO extent of Arp 244. Pointing and focus have been monitored frequently every 1–2 hr by observing nearby quasars 3C279 or 3C273 (and occasionally planets at the beginning of the observations). Uncertainties in positioning are typically \sim 5". Calibration with the standard chopper-wheel method was performed once after every the other 6 minute integration scan and yielded an antenna temperature on a T_R^* scale. Further absolute flux calibrations in the antenna temperature scale have been performed by the repeated observations of the northern nucleus (our map center) during different observing sessions and by the observations of some nearest well-observed starburst galaxies. Comparing the observed line strengths and profiles, we found that the consistency is satisfactory and the difference is less than \sim 20%.

HCN(1-0) was observed in 1997 April at only

two locations: the northern nucleus (NGC 4038) and the CO peaks in the overlap region (Figure 1). This was part of another project to search for the HCN emission in the LIG mergers. Additional integrations at these two locations were obtained in 1999 November as a further consistency check. The 12m telescope’s FWHM beam at 89 GHz (\sim 72"), pointed at the nucleus of NGC 4038, presumably covers all HCN emission in NGC 4038, yet excludes emission from that of NGC 4039 and most of the disk overlap region. The second HCN beam covers not only all the CO peaks and the extended CO in the overlap but also most CO emission in NGC 4039. Therefore, the total HCN emission from Arp 244 can be roughly sampled by simply summing up these two beam measurements. T_{sys} on a T_R^* scale is about 230 K with the dual SIS 3mmlo receivers and the same back ends as used in the CO observations. We have accumulated a total integration time of nearly 5 and 7 hr for NGC 4038 and the overlap/NGC 4039, respectively.

Our data reduction was performed using the CLASS/GILDAS package. Each individual scan was checked for spikes/dips or bad channels and curvatures in the baseline. Scans with the structured baselines have been abandoned, bad channels have been “repaired” by interpolation using the adjacent channels, and a linear baseline was then subtracted after removal of the spikes/dips for each accepted scan. All scans at each same position have then been summed to obtain an average spectrum. The data cubes of the different velocity spacings were also created from the highest velocity resolution (2MHz \sim 5 km s⁻¹) and the smoothed (e.g., 4MHz \sim 10 km s⁻¹) spectra maps. All spectra presented in this paper have been smoothed to 8 MHz (\sim 21 km s⁻¹ for CO and \sim 27 km s⁻¹ for HCN).

3. RESULTS AND ANALYSIS

3.1. Previous CO(1-0) Observations

The currently accepted total molecular gas mass in Arp 244 is based on a single pointing observation with the 12m in the overlap region. Sanders & Mirabel (1985) listed an integrated intensity of 15.9 K km s⁻¹, or a total CO flux of only 556.5 Jy km s⁻¹ (\sim 35 Jy/K on a T_R^* scale), leading to a molecular gas mass of

$2.6 \times 10^9 M_{\odot}$. The Owens Valley Radio Observatory (OVRO) millimeter array's two overlapping field (FWHM $\sim 65''$) CO imaging only recovered $\sim 70\%$ CO flux (Stanford et al. 1990) of the one-beam (FWHM $\sim 55''$) 12m measurement! The 12m beam observed in Sanders & Mirabel (1985) only covered part of the overlap region, neither the nuclear regions of NGC 4038 and NGC 4039 nor the extended structures throughout the entire merging disks (see Figures 1 and 2). Apparently, much of the CO is distributed over a much larger area than the $55''$ beam (Figure 2). Furthermore, the integrated CO line intensity in the old 12m observation was also underestimated owing to the insufficient velocity coverage (Figure 3, more in §3.2).

Young et al. (1995) observed 6 positions in NGC 4038 and one position in NGC 4039 with the Five College Radio Astronomy Observatory (FCRAO) 14m (FWHM $\sim 50''$) and derived a total CO flux of $\sim 2070 \text{ Jy km s}^{-1}$ assuming an uniform CO disk of radius ~ 0.6 for NGC 4038 and an exponential CO disk of a scale-length ~ 0.32 for NGC 4039. Aalto et al. (1995) observed 3 positions in Arp 244 with the Swedish European Submillimeter Telescope (SEST) 15m (FWHM $\sim 45''$), i.e., the overlap region and the nuclear regions of NGC 4038 and NGC 4039. A sum of the integrated CO line intensities from the SEST observations leads to a total CO flux close to what has been estimated by Young et al. (1995). Nevertheless, the new OVRO three-field imaging (Wilson et al. 2000) appears to only recover a total CO flux of 910 Jy km s^{-1} , but this is already more than double that of the old OVRO map of Stanford et al. (1990). All these recent measurements of still very limited spatial coverage have already suggested that the total CO flux in Arp 244 can be a factor of a few larger than what has been previously accepted.

3.2. New CO(1-0) Observations and the Total Molecular Gas Mass

Figure 2 shows all the averaged CO spectra made with the 12m at a half-beam spacing, a total of 73 spectra with more than 50 firm detections. Only CO spectra at the outermost edge generally show non-detection or tentative detections (noted in Table 1). Many CO spectra in the inner part of the map (the disk overlap and

the two nuclear regions) have the integrated line intensities more than $\sim 50\%$ larger than that of the old 12m measurement of Sanders & Mirabel (1985). Observations in 1999 June at the same position as that of Sanders & Mirabel (1985) gave an integrated line intensity exactly twice larger, consistent with those mapped in the nearby positions in 1998 March/April. The northern nucleus was always observed in all observing sessions giving consistent results of about same integrated CO line intensity. Figure 3 presents the three spectra obtained near the CO peaks in the overlap region and compares with the original spectrum of Sanders & Mirabel (1985). Obviously, the old 12m observation may have suffered severely from the poorly determined baseline owing to the limited bandwidth, as the broadest CO spectra in the overlap region have FWZI $\sim 600 \text{ km s}^{-1}$. But, this is probably insufficient to explain a factor of 2 difference in the integrated CO line intensity. Additional errors in the telescope pointing and calibration together with the limited velocity coverage may have all contributed to the discrepancy.

The total CO flux, from our fully-sampled CO observations (summarized in Table 1), is $S_{\text{CO}} dV = 3,172 \pm 192 \text{ Jy km s}^{-1}$ ($I_{\text{CO}} = 90.6 \pm 5.5 \text{ K km s}^{-1}$, using 35 Jy/K conversion for the T_R^* antenna temperature scale), a factor of 5.7 larger than what was initially reported by Sanders & Mirabel (1985). The total CO luminosity is thus $L_{\text{CO}} = 0.3 \times 10^{10} \text{ K km s}^{-1} \text{ pc}^2$ (T_{mb}), or a molecular gas mass $(1.5 \pm 0.1) \times 10^{10} M_{\odot}$ (using the standard CO-to- H_2 conversion factor of $3.0 \times 10^{20} \text{ H}_2 \text{ cm}^{-2} (\text{K km s}^{-1})^{-1}$, or $M(\text{H}_2) = 4.78 \times (L_{\text{CO}} / \text{K km s}^{-1} \text{ pc}^2) M_{\odot}$, applicable to GMCs in the Milky Way disk, e.g., Solomon & Barrett 1991; Young & Scoville 1991). The error estimate is purely from the measurement uncertainties (statistical errors from all measurements and the uncertainties in the CO detections in the outer edge), additional uncertainties up to $\sim 20\%$ should be expected from the calibration and pointing etc.

It is interesting to note that the new estimate of the dust mass in Arp 244, based upon the SCUBA 450 and $850 \mu\text{m}$ measurements as well as the ISOPHOT observations at wavelength longer than $100 \mu\text{m}$, reveals a substantial amount of cold and warm dust, and leads to a total dust mass of $M_{\text{dust}} \sim 10^8 M_{\odot}$ (Haas et al. 2000). Thus, for

a total gas mass of $M_{\text{gas}} \sim M(\text{H}_2) + M(\text{HI}) \sim 1.9 \times 10^{10} M_{\odot}$ [$M(\text{HI}) \sim 4 \times 10^9 M_{\odot}$, van der Hulst 1979; Hibbard et al. 2001 in preparation], a gas-to-dust ratio of $M_{\text{gas}}/M_{\text{dust}} \sim 190$ is obtained. This is basically the same gas-to-dust ratio established in our Galaxy and in some nearby spiral galaxies like NGC 891 (Alton et al. 2000). This simple consistency may also imply that the standard CO-to- H_2 conversion determined from GMCs in the Milky Way disk is likely applicable here and Arp 244 is indeed molecular gas-rich. Table 2 summarizes the global quantities of Arp 244.

3.3. Global Molecular Gas Distribution and Kinematics

Although the most molecular gas is concentrated in the disk overlap region, the extended distribution of the molecular gas spreads essentially all over the merging disks, much further beyond the field of view of the WFPC2 (Figure 2). There are also concentrations of the molecular gas in the two nuclear regions, particularly in the northern one. This is better indicated in the quite coarse channel map of 100 km s^{-1} width (Figures 4a–e). In general, there are good correspondences between the CO distribution and the optical morphology, except for the overlap region where the CO emission appears to be much more prominent than the optical light. Figure 4f further compares the CO integrated intensity contours (using all 74 position CO observations) with the optical disks. All these (Figures 4a–4f) clearly show that the molecular gas extends throughout the system and explain why the old 12m single beam measurement underestimated the total CO emission by a large factor. Obviously, much of the CO over a broad velocity range is simply distributed over several arcminutes, corresponds to a linear CO extent of possibly beyond $\sim 20 \text{ kpc}$.

The deep integration at the SE edge of the overlap region, where the southern tidal tail begins, confirms the clear detections of the weak CO emission from this region (Figure 5a). The central offset of the spectra shown in Figure 5a is ($110''$, $-82.5''$) relative to the northern nucleus, two full beams further out from the peak emission in the overlap region. CO emission is also detected, for example, at offsets of ($55''$, $55''$) and ($81''$, $27.5''$) relative to the northern nucleus, and in a few locations west of the two nuclear regions at one and

half beams from the nuclei (Figure 2 and Table 1). These locations are so far away from the CO emission peaks and their immediately associated CO extensions (also see the new OVRO map of Wilson et al. (2000)), suggesting that there are weak extended CO features across over the entire optical disks. Given the relatively quite strong CO emission and the large distance from the CO emission peaks, it is unlikely that both the pointing errors, as large as $10''$ in some rare occasion, and the telescope beam pattern (sidelobes) can produce such relatively strong CO emission that we have detected near the map edge. This certainly points out the importance of the complete coverage of the merging systems in the single beam observations since they may systematically underestimate the total CO content in the cases where the merging disks are larger than the single beam. A substantial amount of the molecular gas may be distributed at large galactic radii, especially in the young, early and intermediate stage mergers like the “Antennae” galaxies.

The overall velocity spread of the molecular gas is more than 600 km s^{-1} across over the two merging disks. The narrowest velocity ranges are observed in the nuclear region of the northern face-on galaxy NGC 4038 (FWZI $\sim 300 \text{ km s}^{-1}$, FWHM $\sim 100 \text{ km s}^{-1}$), whereas a broader velocity spread (FWZI $\gtrsim 500 \text{ km s}^{-1}$, FWHM $\sim 230 \text{ km s}^{-1}$) can be seen in the southern inclined galaxy NGC 4039. The broadest velocity components (FWZI $\sim 600 \text{ km s}^{-1}$, FWHM $\sim 300 \text{ km s}^{-1}$) are particularly prominent south of NGC 4039 even though the CO emission is quite weak (Figure 2 and Nos. 6, 9, 17, 27, & 29 in Table 1). It is likely that the interferometric observations have almost entirely resolved and thus missed these weak and broad velocity features. The velocity extent around the peak CO emission in the overlap has a similarly broad velocity range. Also, the velocity spread of most spectra in the overlap region lies between the two extremes observed in the two galaxies. This is obvious since some spectra contain the CO contribution from either NGC 4038 or NGC 4039 or both. But, clearly most spectra at a full beam (or more) eastern of the nuclei are basically free from any contribution of the nuclear CO emission. We also notice that, although the difference is small ($\sim 50 \text{ km s}^{-1}$), the systemic velocity in the overlap region is lower

than that of the entire system whereas the systemic velocity south of NGC 4039 is higher. This perhaps reminisces the disk rotation of the molecular gas in the more inclined galaxy NGC 4039. Nonetheless, the average velocities of the molecular gas in the nuclear regions of both galaxies are about same as the systemic velocity of the entire system.

The detailed study of the molecular gas distribution and kinematics is difficult given the limited resolution of the 12m telescope beam, which will be thoroughly described in the presentation of the BIMA + NRAO 12m full-synthesis observations, providing a much improved spatial resolution of nearly 10 times better. Although the enormous amount of molecular gas in the overlap region must originate from both spiral galaxy progenitors, the kinematics and the proximity of the molecular gas in the overlap, combined with the similar velocity spread of the molecular gas motion as that in the southern galaxy NGC 4039, seem to suggest that the most molecular gas in the overlap could be originated from the southern progenitor. The molecular gas content of the two progenitors might be initially comparable and both were gas-rich. However, the VLA HI observations appear to show that the progenitor of NGC 4039 was gas poor since the most HI in this system is currently in the southern tail extending from NGC 4038 (Hibbard et al. 2001 in preparation).

3.3.1. CO in the Southern Tidal Dwarf Galaxy

We have also searched for the faint possible CO emission at several positions in the southern tidal dwarf galaxy (Schweizer 1978; Mirabel et al. 1992) at the tip of the tidal tail. A possible weak CO detection from the beam at position RA=12:01:26.0, Dec=-19:00:37.5 (J2000) appears to be at the $\sim 4\sigma$ level (an integration of more than 12 hr; Fig. 5b). An average of the summed spectra of all observations at the 5 different positions we have searched (accumulated an integration time of more than 27 hr), appears to confirm the weak CO detection at the $\sim 5\sigma$ level. All these observed positions are selected to be around the regions of the highest HI column density, where the VLA HI observations (Hibbard et al. 2000) have revealed some large concentrations of the atomic gas, distributed extendedly around the region of the tidal dwarf galaxy and along the southern tidal tail.

The weak CO detections (Figure 5b) have also shown the same velocity range as the atomic gas velocity spread, revealed from the VLA HI channel maps, further indicating that the weak CO emission is likely real. Yet the much deeper integration and the more observing positions in this region are still required in order to firmly present the CO detections at the very high significant levels, and to possibly obtain a better understanding of the weak CO distribution and kinematics in a tidal dwarf galaxy.

The integrated CO line intensity from the detected position is $I_{\text{CO}} = 0.37 \pm 0.09 \text{ K km s}^{-1}$. The average spectrum of the sum from all other 4 locations (not shown here) appears to give a similar integrated CO line intensity $I_{\text{CO}} = 0.35 \pm 0.12 \text{ K km s}^{-1}$, while the average spectrum of all observations gives an integrated CO line intensity $I_{\text{CO}} = 0.35 \pm 0.07 \text{ K km s}^{-1}$. Earlier observations by Smith & Higdon (1994) failed to detect any CO emission, but our observations here are much more sensitive. Using the standard CO-to-H₂ conversion factor, we therefore obtain a minimum molecular gas mass for the tidal dwarf galaxy $\sim 0.61 \times 10^8 M_{\odot}$ if only the detected position is considered. It is likely that the weak CO emission exists in other locations in this region and the total molecular gas mass for the entire tidal dwarf galaxy can be a factor of several larger. Indeed, the summed average spectrum of all the 5 position observations seems to suggest a molecular gas mass $\gtrsim 2 \times 10^8 M_{\odot}$. Anyway, this molecular gas mass appears to be larger than that of the molecular complexes detected in the M81 group (Brouillet, Henkel, & Baudry 1992; Walter & Heithausen 1999), yet comparable to the molecular gas mass detected in the other two tidal dwarf galaxies (Braine et al. 2000). It is possible that most of the molecular gas might have come directly from the conversion of HI into H₂. This is similar to the case in the two tidal dwarf galaxies where the molecular gas was detected in regions of the highest HI concentrations (Braine et al. 2000), and is also related to the case in the cold intragroup medium where huge HI concentrations and the CO detection are both associated with the intragroup starburst (Gao & Xu 2000) in the famous compact galaxy group Stephan's Quintet.

3.4. HCN(1-0) Detections and the Dense Molecular Gas

The high dipole-moment molecules like HCN, which traces the dense molecular gas at density $\gtrsim 10^4 \text{ cm}^{-3}$, are better tracers of the star-forming gas than that of CO (Solomon et al. 1992; Gao 1996; Gao & Solomon 2000a, 2000b). We have detected the weak HCN(1-0) emission from the two positions, one at the nucleus of NGC 4038 and the other covering both the disk overlap and the nuclear region of NGC 4039 (FWHM $\sim 72''$ at 89 GHz, the two thick circles in Fig. 1). Figure 5c shows the two HCN spectra and the total HCN luminosity can be estimated by the sum of the two beam measurements. This is because, in nearby galaxies where HCN maps exist, the dense molecular gas tends to be concentrated in the innermost disks of the highest density regions (Gao 1996; Helfer & Blitz 1997a). Thus it is unlikely that any significant HCN emission in Arp 244 still exists outside the coverage of the two HCN beams. We estimated the total HCN flux to be $S_{\text{HCN}}dV = 39 \pm 6 \text{ Jy km s}^{-1}$ ($I_{\text{HCN}} = 1.2 \pm 0.2 \text{ K km s}^{-1}$, using a $\sim 32 \text{ Jy/K}$ conversion) and the HCN luminosity $L_{\text{HCN}} = 0.7 \times 10^8 \text{ K km s}^{-1} \text{ pc}^2$. Therefore, the luminosity ratio of $L_{\text{HCN}}/L_{\text{CO}} = 0.02$ implies only $\gtrsim 5\%$ of the molecular gas is at high density of $\gtrsim 10^4 \text{ cm}^{-3}$ in Arp 244 (Gao 1996; Gao & Solomon 2000a). This is surprisingly low since ULIGs can have as high as $L_{\text{HCN}}/L_{\text{CO}} = 0.25$ and up to about half of the molecular gas at density $\gtrsim 10^4 \text{ cm}^{-3}$ (Solomon et al. 1992; Gao 1996; Gao & Solomon 2000a). The ratio of $L_{\text{HCN}}/L_{\text{CO}}$ in Arp 244 is actually just comparable to that of the Milky Way disk (Helfer & Blitz 1997b), even lower than that of some “normal” spiral galaxies (Gao & Solomon 2000a). The fraction of the dense molecular gas in Arp 244 is apparently the lowest among all LIGs observed so far.

Although most of the CO emission ($\gtrsim 60\%$) is from the overlap region, the HCN emission in the overlap appears to be less than half since only about half of the HCN emission is originated from both NGC 4039 and the overlap. The HCN detection from the overlap region and NGC 4039 has only a comparable integrated line intensity, but weaker in the antenna temperature as compared with the detection in NGC 4038. The two HCN spectra differ clearly in the velocity spread: a narrow velocity space in the HCN emission of

NGC 4038 whereas a much broader velocity spread in NGC 4039 and the overlap region. Thus, the HCN spectra basically indicate that the dense molecular gas could have the similar gas kinematics as that of the total molecular gas revealed from the CO emission even though their spatial distributions are probably totally different.

The low fraction of the dense molecular gas in Arp 244, especially in the overlap region, is consistent with the fact that the bulk of the molecular gas in the overlap is extensively distributed both spatially and kinematically (Figs. 2, 3 and 4). Although there are several CO peaks in the high resolution synthesis maps, none of them has the extremely high concentrations of molecular gas as those found in ULIGs. The highest gas surface density in the northern nucleus is $\sim 2.5 \times 10^3 \text{ M}_{\odot} \text{ pc}^{-2}$ (resolved on a linear scale of $\sim 0.5 \text{ kpc}$ as in both the BIMA plus NRAO 12m and the new OVRO CO maps), order of magnitude smaller than those in ULIGs, whereas the gas surface density in the southern nuclear region is lower by at least a factor of 3 and comparable to that of the CO peaks in the overlap. Our low-resolution ($55'' \sim 5 \text{ kpc}$) 12m map reveals a CO peak in the disk overlap region since most of the molecular gas is concentrated there. The peak molecular gas column density $N(\text{H}_2)$ is close to 10^{22} cm^{-2} , i.e., an average gas surface density (over $\sim 5 \text{ kpc}$ scale) of about $190 \text{ M}_{\odot} \text{ pc}^{-2}$. This low gas surface density together with the low HCN-to-CO line luminosity ratio clearly marks the unique gas properties in Arp 244, in sharp contrast with those in most LIGs/ULIGs.

3.5. Local Star Formation Efficiency and the Radio-to-CO Ratio Map

There is apparently a correlation between the radio continuum and the CO emission as even so indicated in the old OVRO CO map (Hummel & van der Hulst 1986; Stanford et al. 1990). Particularly, most of the radio continuum emission is extensively concentrated in the overlap region with a very similar morphology to that of the CO. The direct comparison of the *KAO* $60 \mu\text{m}$ maps (Evans et al. 1997) with our full-synthesis CO images clearly reveals that the average FIR to CO ratio in the overlap region is higher than the global ratio since most of the FIR emission ($\gtrsim 75\%$) is from the overlap region, whereas only $\gtrsim 60\%$ CO emission

is from the same region. Therefore, the average SFE in the overlap can be a bit higher than the global value (which is $L_{\text{IR}}/M(\text{H}_2) = 4.2 L_{\odot}/M_{\odot}$, or $5.3 L_{\odot}/M_{\odot}$ if a higher $100 \mu\text{m}$ KAO flux of Bushouse et al. (1998) is used), still comparable to that of GMCs in the Galactic disk and an order of magnitude lower than that of ULIGs (Sanders & Mirabel 1996; Solomon et al. 1997). On the other hand, the average SFE in the nuclear regions is expected to be lower than the global value since the two nuclear regions have extremely weak FIR emission, whereas the CO is highly concentrated, particularly in NGC 4038. Moreover, the radio continuum emission has indeed an excellent correspondence with the FIR maps, just as expected from the well-known correlation between the radio continuum and the FIR emission (e.g., Helou et al. 1985; Marsh & Helou 1995).

In order to further quantify the local star formation properties and better identify the sites of the most intense starbursts with the highest SFE, we have produced the ratio map of the VLA 20cm radio continuum to the CO(1-0) emission. Since the tight FIR/radio correlation is also valid on kpc scale in galaxies (e.g., Marsh & Helou 1995; Lu et al. 1996), the radio continuum emission can be used as a tracer of the recent star formation in galaxies as well (e.g., Condon et al. 1990, 1991; Condon 1992). We here use the radio continuum maps to roughly indicate the star formation sites. Thus, a high resolution indicator of the FIR emission can be inferred by scaling the FIR according to the radio continuum emission. Comparing the radio continuum maps with the detailed molecular gas distribution from the CO imaging, we can obtain the radio-to-CO ratio map to reveal the local SFE, which is defined as the local ratio of the star formation rate to the molecular gas mass. Both the VLA 20cm continuum and the BIMA plus the NRAO 12m full-synthesis CO maps have about same resolution, thus a direct division can be performed to obtain the ratio map.

The radio continuum to the CO ratios have been plotted as contours and compared with the HST/WFPC2 (Fig. 6) and the VLA radio continuum images (Fig. 7). Apparently, a rather smooth distribution of the radio-to-CO ratio is observed across over most of the merging disks. The sites of the highest ratios, ~ 2.5 and 5 times above the average, have been indicated in Figure 6 as

black and white contours, respectively, and they coincide well with the dusty patches across over the HST/WFPC2 image. The sites of the highest radio-to-CO ratios are exclusively localized in the most prominent dusty regions in the overlap, which are near the CO peaks and probably the FIR emission peaks. The correspondent highest SFE is therefore $\gtrsim 20 L_{\odot}/M_{\odot}$ since the global average SFE is $4.2 L_{\odot}/M_{\odot}$. Interestingly, almost all LIGs/ULIGs have SFE $\gtrsim 20 L_{\odot}/M_{\odot}$ (Sanders & Mirabel 1996), although some early stage pre-merging LIGs with SFE $\sim 10 L_{\odot}/M_{\odot}$ and lower do exist (e.g., Arp 302, Lo, Gao, & Gruendl 1997).

Consistent with what can be roughly expected from a direct comparison of the FIR map at $60 \mu\text{m}$ with the CO images in the nuclear regions, both nuclei have only a low radio-to-CO ratio, about the average or lower (Fig. 7). Thus the SFE in the nuclear regions is about $4 L_{\odot}/M_{\odot}$. The *ISO* MIR “hotspots” have higher ratios than the average, so do the extended overlap region and the western star-forming loop in NGC 4038, in addition to a few spots around the nuclear regions (especially the circumnuclear region of NGC 4038, Fig. 6). But these are a factor of 2 lower than the highest ratios and are only of moderate starburst sites with a SFE $\gtrsim 10 L_{\odot}/M_{\odot}$, which is actually the typical SFE value for the local starburst galaxies (Sanders & Mirabel 1996).

4. DISCUSSION

Both observational and theoretical studies have demonstrated that the ultraluminous extreme starburst phase is most likely achieved in the molecular *gas-rich* mergers (e.g., Sanders & Mirabel 1996; Mihos & Hernquist 1996; Downes & Solomon 1998; Gao & Solomon 1999) where starbursts may proceed through the formation of numerous super-star clusters (e.g., Whitmore et al. 1999; Surace et al. 1998; Scoville et al. 2000). Multiwavelength observations of Arp 244 and comparison with the early stage mergers observed by Gao et al. (1999) are therefore especially crucial to track how and when the dominant sources of star formation transform from within the disks of the two *gas-rich* spirals to the disk-disk overlap regions between the two galaxies. Moreover, comparative study with CO observations of the late stage mergers (Downes & Solomon 1998;

Bryant & Scoville 1999) are also equally important for understanding how the starbursts continue to evolve from taking place predominantly in the overlap regions to occurring mainly in nuclear regions when the merging advances to ULIG phase, with extraordinary nuclear concentrations of dense gas. Intermediate mergers like Arp 244 serve apparently as an important link in the merging process between a pair of gas-rich premergers and the merged double-nucleus ULIG. We here discuss only the starburst properties of Arp 244 related to our 12m observations.

4.1. Ultraluminous Extreme Starburst Potential

The CO content is decreasing as merging progresses, indicating the depletion of molecular gas due to merger-induced starburst (Gao & Solomon 1999). Using the scaling of $M(\text{H}_2) \sim S_{\text{sep}}^{0.8}$ (Gao & Solomon 1999, valid for mergers at the early and intermediate stages, with the projected nuclear separation $20 \gtrsim S_{\text{sep}} \gtrsim 2$ kpc), the total molecular gas will decrease roughly by more than a factor of 2 when Arp 244 reaches $S_{\text{sep}} \sim 2$ kpc, prior to or about entering into the late merging stage. It appears that all ULIGs observed so far have $\sim 10^{10} M_{\odot}$ of molecular gas mass or more without exception, even after considering up to a factor of 5 reduced CO-to- H_2 conversion (Solomon et al. 1997). The ultraluminous starburst phase of Arp 244 is thus possibly reachable in the advanced stage since only $\sim 10^{10} M_{\odot}$ molecular gas will be consumed by the newborn stars in the next $\sim 10^8$ yr of the merging process. There will still be abundant molecular gas of close to $\sim 10^{10} M_{\odot}$ available, not to mention the additional amount of atomic gas in the merging disks and in the long tidal tails (Hibbard et al. 2001 in preparation) that may eventually fall back to the merging disks (Hibbard et al. 1994). The atomic gas could be an additional gas reservoir for possible conversion into the molecular phase, because there appears to be some evidence that ULIGs tend to have the highest ratio of $M(\text{H}_2)/M(\text{HI})$ (e.g., Mirabel & Sanders 1988, 1989).

In general, the gas surface density increases from orders of a few times $10^2 M_{\odot} \text{pc}^{-2}$ to a few times $10^3 M_{\odot} \text{pc}^{-2}$, as merging progresses from early to intermediate stages (Gao et al. 1999) (unresolved on a scale of 1–2 kpc), whereas

advanced ULIG mergers such as Arp 220 have gas surface density typically greater than $10^4 M_{\odot} \text{pc}^{-2}$ (Scoville et al. 1997; Downes & Solomon 1998; Sakamoto et al. 1999). Although the total molecular gas content of Arp 244 is comparable to that of ULIGs, the gas surface density is still orders of magnitude lower than that of ULIGs, e.g., in the overlap, $\sim 10^2 M_{\odot} \text{pc}^{-2}$ on a scale of 5 kpc and $\sim 10^3 M_{\odot} \text{pc}^{-2}$ on a resolved scale of sub-kpc. Therefore, only a small fraction of the molecular gas in Arp 244 is actually at a high enough gas surface density for a high SFE, as formulated in the Schmidt law (e.g., Kennicutt 1998). The overall gas density is low to maintain a low SFE across over the entire system, except for some localized starburst regions (Fig. 6), just as our HCN observations have revealed that little dense molecular gas available currently to power the extreme starbursts.

Ultraluminous extreme starbursts require not only a large quantity of molecular gas but also a high gas concentration, particularly the nuclear gas concentration, so that the bulk of the molecular gas is at a high density. The large quantity of pre-existing molecular ISM is the sufficient fuel for Arp 244 to ultimately reach the onset of the ultraluminous starburst phase, as the merging proceeds to the advanced stage, and the bulk of the molecular gas becomes highly condensed. Unlike most LIGs/ULIGs, which show the dominant nuclear MIR and perhaps FIR emission (Hwang et al. 1999; Soifer et al. 2000; Bushouse et al. 1998; Xu et al. 2000), Arp 244 has only moderate nuclear emission in MIR (Mirabel et al. 1998; Xu et al. 2000), and the *KAO* 60 μm emission from the two nuclei is extremely weak (Evans et al. 1997). Although there is no clear indication of a large stellar bulge in either of the galaxies, the concentrations of the molecular gas as well as the stars in the nuclear regions in Arp 244 perhaps also draw some analogies to the case of galaxy-galaxy merger model with stellar bulges in the progenitors (Mihos & Hernquist 1996). In reality, Arp 244 is probably more in between the two extreme cases modeled by Mihos & Hernquist (1996). According to the models (see Figure 5 in Mihos & Hernquist 1996), the first peak of starburst phase has recently passed in Arp 244, shortly after the pair's first closest approach, perhaps as evidenced by numerous young star clusters in the HST/WFPC2

images. Thus, Arp 244 could have just phased out the bona fide starburst LIG stage. As more and more gas continues to accumulate in both the overlap and the two nuclear regions, the further nuclear gas concentrations and the continuous star formation can build stronger bulges that can help stabilize the disks against the bar formation, lower the SFE levels during the merging, and leave enough gas for the strongest final starburst when the two galaxies eventually coalesce, with almost all the molecular gas collapsed into a kpc double-nucleus region. More than an order of magnitude increase in the SFE, combined with an abundant molecular gas supply of $\sim 10^{10} M_{\odot}$, will be just sufficient to make Arp 244 into $L_{\text{IR}} \sim 10^{12} L_{\odot}$. Interestingly, there also appears to be some quite widely separated ULIGs ($S_{\text{sep}} > 10$ kpc), which might still be in their early stage of merging, but may have passed their first closest impacts, and may have just been experiencing their first strongest starbursts (Murphy 2000).

In summary, a preexisting abundant molecular gas content is a necessary for there to be a possibility of a merging spiral pair reaching the ultraluminous starburst phase. Arp 244, with a large quantity of molecular gas available at low density, a low SFE, a moderate FIR luminosity or star formation rate, and yet a relatively early/intermediate stage of merging, has the potential of producing an ultraluminous extreme starburst in late stage of merging, when the molecular gas complexes in the overlap region eventually merge with the nuclear gas concentrations and finally collapse into a kpc-scale double-nucleus gas disk.

4.2. Starbursts and the Current Intense Star Formation Sites

The well-known correlation between the FIR thermal dust emission and the radio continuum synchrotron emission, unexpected as they are apparently two unrelated physical mechanisms, is probably the tightest relation known among the global quantities of galaxies (e.g., Helou et al. 1985; Condon 1992; Xu et al. 1994). The morphologies of the two emission are also similar and the correlation between them appears to hold down to kpc scale within individual galaxies (e.g., Bica, Condon, & Helou 1989; Marsh & Helou 1995; Lu et al. 1996). Based on these, we approximately scaled the local FIR emission according to

the radio continuum emission, and compared with the molecular gas distribution to measure the local SFE. We have clearly identified that the most intense bursts of star formation (the sites of the highest SFE, i.e., the highest radio-to-CO ratios, Figure 6), currently being observed, are not in the concentrations of the optically revealed star clusters, or even the peaks of the MIR emission, nor necessarily at the exact locations of the CO and 20cm radio continuum emission peaks. Instead, the strongest starbursts appear to be confined in small regions near the CO, radio continuum, and FIR emission peaks in the overlap region. The bulk of the molecular gas across over the entire system is making stars with a rather modest or “normal” SFE (Fig. 7).

Let us emphasize what we have learned from our observations and the various other observations. Starbursts have apparently been going on or happened in some regions in Arp 244 as evidenced by super-star clusters (Whitmore et al. 1999) and the MIR “hotspots” in the overlap (Mirabel et al. 1998). Yet, most of the FIR emission (as well as the MIR), which dominates the total energy output, comes from the overlap region (Evans et al. 1997; Bushouse et al. 1998), where most molecular gas resides, rather than from the super-star cluster concentrations. Although Arp 244 has long been claimed as the nearest archetypal starburst merger, our observations show that the molecular gas is rather extensively distributed over the entire merging disks, though most is still in the overlap, and the bulk of the molecular gas is only making stars at a low SFE. The entire system is presently not undergoing a global burst of star formation, even though some localized starbursts are occurring in the overlap, and a global starburst could have just peaked recently, right after the first closest impact responsible for the formation of the tidal tails.

Whitmore et al. (1999) found that the star clusters at the edge of the dusty overlap region appear to be the youngest, with ages $\lesssim 5$ Myr, while the star clusters in the western loop in NGC 4038 appear to be 5-10 Myr old. Indeed, these are the sites of the most intense and moderate starbursts respectively as revealed by the radio-to-CO ratio map in Figure 6. There might be many youngest star clusters totally obscured by the dust at the most intense starburst sites, contributing signifi-

cantly to the dominant energy output in the overlap region. On the other hand, many star clusters in the northeastern that appear to be ~ 100 Myr old, and even older star clusters across over the system, are not the current starburst sites, contributing little to the total FIR emission. These old star clusters are probably related to the recent large-scale active star formation happened after the first closest encounter.

The excellent agreement among the sites of the highest radio-to-CO ratios, the dark patches in the HST/WFPC2 images, and the youngest ages of the star clusters, is striking. Apparently both the most intense localized starbursts and the overall large-scale star formation are occurring in the overlap region, where all the CO, [C II] line (Nikola et al. 1998), FIR, and radio continuum show high concentrations. But, the confined intense starburst sites, which are heavily obscured in the dust, have only SFE $\gtrsim 20 L_{\odot}/M_{\odot}$, just reaching the typical SFE level for LIGs/ULIGs. On the other hand, the average SFE in the overlap is just slightly larger than $4 L_{\odot}/M_{\odot}$, still comparable with that of the Galactic disk GMCs.

One caveat is that Arp 244 may be twice luminous in $100 \mu\text{m}$, as measured by the KAO (compared with that of the *IRAS* measurement, Bushouse et al. 1998), although the $60 \mu\text{m}$ measurements agree (Evans et al. 1997). This discrepancy needs future FIR observations to resolve. More importantly, it is perfectly possible that the standard CO-to- H_2 conversion factor can be an overestimate for the total molecular gas mass. Therefore, it is likely that the global SFE in Arp 244 can be up to more than a factor of 2 larger than that of the GMCs in the Milky Way disk. This may indeed suggest that an enhanced global SFE proceeds throughout the entire merging disks while some confined strongest starbursts have a highest SFE much larger than $20 L_{\odot}/M_{\odot}$, typical for ULIGs. In any case, the highest radio-to-CO ratio sites could actually be bona fide sites of the *current* starbursts with an elevated SFE, and may contribute a significant fraction to the total FIR emission, even though most of the FIR emission may still come from the regions of a normal or modest SFE.

Using the [C II]/CO(1-0) line ratio to distinguish between starburst activity in galaxies and more quiescent regions (Stacey et al. 1991), Nikola

et al. (1998) concluded that there is no strong starburst activity taking place in Arp 244 on a scale of ~ 5 kpc, the resolution of their data. This is roughly in agreement with our results since starburst sites are only identified on a scale of $\lesssim 1$ kpc (Fig. 6). Nikola et al. (1998) further argued that most of the [C II] emission might have come from the confined active star forming regions surrounded with the more quiescent GMCs. Our results appear to support this claim if indeed the sites of the intense starbursts, which are identified from the high radio-to-CO ratios (Fig. 6), are producing the bulk of the [C II] emission. Additional supports for the confined starbursts in small regions in the overlap are the recent ISO-SWS measurements (Kunze et al. 1996) and the ISO-LWS observations, including the detection of Br γ knots in the overlap interaction zone (Fischer et al. 1996).

The rather extended moderate starbursts also coexist closely with the confined, most intense starbursts in the overlap region. Other interesting sites of moderate starbursts are the western loop/ring structure, and part of the \gtrsim kpc scale circumnuclear regions (mainly in NGC 4038), but not the nuclei themselves (Figs. 6 & 7), with nearly 3 times higher SFE than the average. The western loop coincides with the molecular ring we have mapped from the BIMA plus the NRAO 12m full-synthesis CO image, which was completely absent from the old OVRO CO map (Stanford et al. 1990), and was only partially revealed in the new OVRO CO map (Wilson et al. 2000). It appears that the starbursts occur at a moderate level in the southeast side of the overlap region, proceed progressively with increased intensity towards northwest across over the overlapping molecular concentrations, and produce the most vigorous starburst in the northern and western edges of the huge molecular gas agglomerations in the overlap interaction zone (Fig. 7).

Moderate [C II] emission is also detected in the western loop (Nikola et al. 1998), which also indicates the moderate star-forming activity there. This is again consistent with our results obtained from the radio-to-CO ratios. Moreover, the [C II] emission peak appears to be slightly offset from our single-dish CO peak (Figures 2 & 4f), which is resolved into several CO peaks by the interferometers. The strongest [C II] emission seems to

be roughly coincident with the sites of the highest SFE, just north of the CO peak in the NRAO 12m map. Our single-dish CO map also appears to be roughly peaked at same position as that of the KAO 60 (Evans et al. 1997), 100 and 160 μm maps (Bushouse et al. 1998). The strongest MIR peak in the overlap region that is inconspicuous at optical wavelength (Mirabel et al. 1998; Xu et al. 2000), however, may correspond only to the southernmost CO peak in the overlap (Wilson et al. 2000), which is not one of the strongest starburst sites and has only a moderate SFE $\gtrsim 10 L_{\odot}/M_{\odot}$ (Figures 6 & 7). Therefore, the strongest peaks of the CO, radio continuum, and FIR, as well as the MIR peaks, are not necessarily the exact sites of the highest SFE, or the most intense starbursts. The highest radio-to-CO ratio peaks, which may reveal the sites of the most vigorous star formation with the highest SFE, and the strongest [C II] emission peaks, which arise mainly from the photodissociation regions, appear to be the best probes of the most intense starbursts, which might be totally obscured in the optical/near-IR and even in the MIR regime.

4.3. Star Formation from the Multiwavelength Observations

In light of the numerical models for mergers of Arp 244 alike (Toomre & Toomre 1972; Barnes 1988; Mihos et al. 1993; Mihos & Hernquist 1996; Barnes & Hernquist 1996, 1998) and the multi-wavelength observations of Arp 244, comparison of the various observations and statistical studies of LIG mergers with those models can be fruitful. We here try to discuss qualitatively the onset of the starbursts, the fate of the starbursts, and the possible ultraluminous extreme starburst phase in Arp 244, utilizing these observational and theoretical results.

ROSAT high-resolution imager (HRI) X-ray map (Fabbiano et al. 1997) and the high-resolution and high-sensitivity Chandra X-ray images from the Chandra news release (Fabbiano et al. 2000), after the submission of this paper, show some correspondence with the discrete radio knots. Most soft X-ray emission, however, is from the disks and nuclear regions, rather than from the overlap region, even though several X-ray emission knots exist in the overlap. Yet, more soft X-ray structures in regions of the *ISO* “hotspots” are

evidently better revealed in the new Chandra X-ray images. Both the X-ray and radio continuum show extended morphology (prominent ring structure) in the northern galaxy NGC 4038, though not in NGC 4039. Since supernova remnants are most likely responsible for the majority of both extended emission, these observations may be used as probes to identify *past* active star formation sites. According to the various models, the first burst of star formation may have occurred several $\sim 10^8$ years ago when the first closest approach of the galaxy pair happened. Many X-ray knots with the radio emission correspondence can be even older, and they are reminiscent of the possible star forming sites in the past, prior to or during the first strongest impact. Overall, these emission could mark roughly the sites of the interaction enhanced large scale star formation across over the pair’s disks at the earliest stage of merging.

H α emission and young star clusters shown in the HST images (Whitmore et al. 1999) indicate that recent vigorous star formation is also proceeding throughout the entire merging disks. Molecular gas concentrations in the overlap may have hidden some extremely young star clusters and HII regions. Nevertheless, these again are the rather *recent* large scale bursts of star formation occurring probably right after the genesis of the tidal tails, after the pair’s first closest approach.

Both the MIR and FIR observations (Mirabel et al. 1998; Xu et al. 2000; Evans et al. 1997; Bushouse et al. 1998) show the strongest peaks in the rather extended overlap region where the bulk of the molecular gas resides. But the MIR and FIR emission peaks differ from each other, whereas the FIR peaks roughly at same position as that of the CO. Generally speaking, the overlap region is the *current* sites of vigorous star formation or starburst. Yet, the overall starburst level is at most modest. The strongest starburst sites with SFE comparable to that of LIGs/ULIGs are confined to \lesssim kpc scale small regions in the overlap, and the global SFE level is about same as those in the Milky Way disk GMCs. Despite some localized starbursts are still going-on, the recent peak of starburst phase in Arp 244 has most likely passed already, and the entire system is currently in a rather quiescent star formation phase.

The radio continuum-to-CO ratio map implies low SFE at both nuclei (Fig. 7). The highest gas

concentration in Arp 244 revealed by the interferometers is, however, in the northern nuclear region, which has only moderate \gtrsim kpc scale circumnuclear starburst ring, rather than a sub-kpc nuclear starburst. The highest radio-to-CO ratios are the confined bona fide starburst sites (Fig. 6) which appear to have some correspondence with the [C II] emission peaks (Nikola et al. 1998). The CO emission peaks in the overlap region appear not to be at the exact locations of the localized starbursts, and the most intense starbursts might not be at an extremely high SFE level as in ULIGs. These highest molecular gas concentrations are likely to undergo *future* ultraluminous extreme starburst once they all merge together with the nuclear gas concentrations, and collapse into \sim kpc scale in the final coalescence. Although the progenitor galaxies of Arp 244 could only have small stellar bulges, the bulges can be built up through merging (e.g., Carlberg 1999) in addition to nuclear gas infalls and concentrations. Thus, Arp 244 fits most likely between the two extremes modeled by Mihos & Hernquist (1996), and more than an order of magnitude enhanced SFE can be achieved in the final merging.

Although most (\gtrsim 60%) HI gas is distributed in the tidal tails (van der Hulst 1979; Hibbard et al. 2000), there are still $\sim 2 \times 10^9 M_\odot$ HI in the merging disks, whereas most ULIGs have little HI left in the merged disks (Hibbard & Yun 1996, 2000; Mirabel & Sanders 1988, 1989). Most HI in Arp 244 is in the southern tail, where we tentatively detected CO emission at the tip of the tidal tail, indicating a molecular gas mass of $\gtrsim 2 \times 10^8 M_\odot$ in the tidal dwarf galaxy. These are additional gas reservoir for *future* star formation, especially when the extraordinary HI tails rain back onto the merging disks (Hibbard et al. 1994), converting most HI gas into molecular phase.

Our recent HI observations of NGC 6670 suggest that a precursor to Arp 244 can be that the HI disks have merged into a huge overlap concentration in the extended HI disks, prior to the merging of the stellar and molecular gas disks (Wang et al. 2000). In Arp 244, although an anti-correlation between the molecular and atomic gas distributions appears to exist, there is still a significant amount of HI gas in the molecular gas overlap region. Whether there was a HI gas overlap formed previously, prior to the merging of the molecu-

lar gas disks, requires high resolution HI observations and further comparative studies of the multi-wavelength observations, in combination with the numerical modelings, to test. Clearly, understanding of the formation and evolution of the overlap region is the key to ultimately comprehend the entire star formation history of Arp 244.

4.4. Overlap Star Formation and Starburst Mechanisms

The formation of the overlap star formation regions, unnecessarily as overwhelmingly dominant as in the case of Arp 244, might be a quite common phenomenon in merging galaxies (Xu et al. 2000). Both the simulations and observations have shown that the gas is being transported into the nuclear regions when a pair of spiral galaxies undergoes through the merging process, in addition to being dragged out into the tidal tails (e.g., Olson & Kwan 1990a,b; Noguchi 1991; Mihos & Hernquist 1996; Barnes & Hernquist 1991, 1996; Scoville et al. 1991; Gao et al. 1999; Hibbard & van Gorkom 1996). Yet, models appear to be unable to reveal the early formation of the gas concentration in the overlap region when galaxies are still quite widely separated, like the intermediate merger Arp 244 with the molecular gas overlap, where most gas resides, and the early merger NGC 6670 with the atomic gas overlap. Could a significant amount of the atomic gas, especially in the southern progenitor, have ended up in the overlap region in the first place, prior to the formation of the molecular gas overlap, as a result of efficient HI cloud-cloud collisions than the collisions of the GMCs, when the two gas-rich spiral progenitors first collided? This is because the mean free path of a HI cloud is ~ 33 pc, much smaller than the size of the overlap region, yet the GMCs' mean free path is orders of magnitude larger and the chance of GMC collisions in the overlap is extremely small (Jog & Solomon 1992). Just like the early merger NGC 6670, which has the HI gas concentration in the HI disk overlap region formed prior to the merging of the stellar and molecular gas disks (Wang et al. 2000), there might be a similar HI gas overlap formed in Arp 244 during its earliest merging stage.

Jog & Solomon (1992) argued that a starburst occurs when the preexisting GMCs in the overlap region undergo radiative shock compressions by

the preexisting high pressure of the central molecular intercloud medium produced by the heating from the HI cloud-cloud collisions. If indeed an HI disk-disk overlap region could be formed prior to the merging of the stellar and molecular gas disks, the dominant star formation should not be occurring in the HI gas overlap region, given few GMCs exist in this HI cloud-cloud collision ISM during the early stage of merging. Instead, large-scale star formation and nuclear starbursts induced by the gas inflow are probably at play (Combes et al. 1994). It is later formation of the molecular gas disk overlap, within this preexisting high pressure overlapping HI gas concentration, when the merging advances into the intermediate stage, that will probably make GMCs in the overlap undergo starburst by the radiative shock compressions (Jog & Solomon 1992).

Although the soft X-ray emission in the overlap region in Arp 244 is neither strong nor extended, as revealed by the ROSAT HRI (Fabbiano et al. 1997), this may be due to the high gas column density in the overlap which absorbs the most extended soft X-ray emission. The Chandra soft X-ray images of much improved sensitivity and resolution do show some extended features in the overlap, which are particularly in good correspondence with the MIR “hotspots”. This is in the right track, just as expected from the prediction of the overlap starburst model of Jog & Solomon (1992). Higher energy X-ray imaging that can penetrate through the heavy dust/gas concentration in the overlap, yet still orders of magnitude below the Compton-thick limit, and the extinction-corrected soft X-ray images of Arp 244 could be the key to further test the overlap overpressure starburst mechanism.

In advance mergers, the double-nucleus gas disks are already merging with the overlap gas concentrations, with most gas either between (e.g., NGC 6240, Tacconi et al. 1999) or around the double-nucleus (e.g., Arp 220, Downes & Solomon; Sakamoto et al. 1999) in \sim kpc scale, in addition to the nuclear gas concentrations. Thus, a possible merging sequence for a gas-rich pair of spirals may look like the following: from the build-up of the HI gas disk overlap regions (NGC 6670) \rightarrow the sufficient overlap in both stellar and molecular disks (Arp 244) \rightarrow the kpc scale merging double-nucleus gas disks, either with a central gas concentration

between the nuclei (NGC 6240), or with an extended gas disk of several kpc surrounding the nuclei (Arp 220). The transformation of the merging phases and the further development of the overlap regions are also accompanied by the change in the dominant sources of the total power output: from large scale star formation within galaxy disks in early mergers \rightarrow the mainly localized starbursting overlap regions between the galaxies in intermediate mergers \rightarrow the extreme starburst in the highly concentrated double-nucleus sub-kpc sources in advanced ULIGs.

The overpressure starburst mechanism (Jog & Solomon 1992) is probably happening in intermediate mergers, especially those with the extensive overlap regions like Arp 244. Yet, this mechanism appears to require a sufficient overlap between the gas disks so that the early formation of the gas overlap region is possible. Is this the sole starburst mechanism during the entire merging process when two gas-rich spiral galaxies merge? It is likely that different starburst mechanisms play various roles during different merging stages along a merger sequence. What then are the other triggering mechanisms for the starbursts? Wilson et al. (2000) compared their new OVRO CO map with the *ISO* MIR emission and suggested that molecular cloud collisions may play an important role for the local intense starburst and the strong MIR emission. Yet, Lo et al. (2000) found no obvious signatures of cloud collisions from analyzing the molecular gas kinematics in the BIMA + the NRAO 12m full-synthesis CO data. Perhaps Arp 244 is on its way of changing from the overpressure overlap starburst to the direct cloud-cloud collision starburst.

An extensive active star forming molecular gas overlap region observed in Arp 244 may not always be the case for most mergers. In fact, most LIGs do not show such an extensive molecular gas overlap region (e.g., Gao et al. 1997, 1999; Bryant & Scoville 1999). Even though star formation in the overlap can be common in mergers, the overlap starburst is probably much less dramatic than that of Arp 244 in most cases (e.g., Xu et al. 2000). But, do all gas-rich mergers develop such an extensive molecular gas overlap phase during the course of merging? We do not have a definite answer. Only in late merging stage have both observations and numerical simulations demonstrated the exist-

tence of the highly concentrated molecular gas between the merging nuclei. Also, only in advanced mergers, can the chance of GMC-GMC collisions be much enhanced since almost all the molecular gas (in both the overlap and the two nuclear gas concentrations) finally condenses into a kiloparsec scale. Now, the mean free path of GMCs is less than the size scale of the gas concentration region since the volume filling factor of GMCs is ten-fold increased, making even the intercloud medium molecular. Therefore, direct collisions of GMCs could be playing an important role for the enhanced starburst when merging progresses into advanced stage in the final coalescence.

5. CONCLUSIONS

We summarize our main results and present our concluding remarks in the following:

1. Our fully sampled CO(1-0) map (FWHM $\sim 55''$) at half-beam spacing reveals a factor of 5.7 larger total CO flux in Arp 244 than the previously accepted. This is mainly due to the enormous CO extent of Arp 244, which is much larger than the single pointing $55''$ beam used in the old observation. In general, single beam observations of merging systems may well systematically underestimate CO content in the cases where the merging systems are much larger than the single beam, unless a map of extensive coverage of the merging systems is made. Most of CO emission in Arp 244 indeed peaks at the disk overlapping region with a broad velocity spread of 600 km s^{-1} . We obtain a total molecular gas mass of $1.5 \times 10^{10} M_{\odot}$ for Arp 244 using a standard CO-to- H_2 conversion factor.

2. HCN(1-0) emission has been detected in Arp 244. HCN observations suggest that there is only a small amount of dense molecular gas in Arp 244 compared to the total molecular gas content. The fraction of the dense molecular gas is only comparable to that of normal spiral galaxies and is much lower than that of luminous and ultraluminous infrared galaxies (LIGs/ULIGs).

3. We detected extended CO emission far away (nearly two full beams) from the major CO concentrations, such as those revealed by the interferometers. The peak CO emission in the overlap region has an average gas surface density near $\sim 200 M_{\odot} \text{ pc}^{-2}$ over $\sim 5 \text{ kpc}$ — the scale probed

by the $55''$ beam. Even the resolved interferometry CO images only reveal that the highest gas surface density is about $10^3 M_{\odot} \text{ pc}^{-2}$, still order of magnitude lower than that of ULIGs. This is consistent with the small fraction of dense gas found from the HCN measurements. Weak CO emission from the tidal dwarf galaxy at the tip of the southern tail has also been tentatively detected and the estimated molecular gas mass is possibly larger than $\sim 2 \times 10^8 M_{\odot}$.

4. The excellent correspondence of the radio continuum images with the FIR maps is evident in Arp 244, which also implies the tight correlation between the two emission. We use the high resolution VLA 20cm image to approximately represent the FIR emission distribution in Arp 244, and compare with the CO images of comparable resolution to estimate the local star formation efficiency (SFE), which is defined as the FIR to molecular gas mass ratio, and is now indicated by the radio-to-CO ratio. SFE is low throughout the entire system with a global SFE = $4.2 L_{\odot}/M_{\odot}$, just same as that of the Galactic disk GMCs. Only some confined regions in the overlap, inconspicuous in optical observations, are the sites of the current powerful starbursts with SFE $\gtrsim 20 L_{\odot}/M_{\odot}$, comparable to that of LIGs/ULIGs. The VLA radio continuum images also reveal a very similar morphology as that of the molecular gas distribution.

5. Although some localized starbursts are going on in the confined regions in the overlap, the bulk of the molecular gas is forming into stars with a low SFE, just same as that of normal spiral galaxies. The large amount of total molecular gas, yet only a small amount of dense molecular gas and a low SFE, revealed from our observations, combined with the theoretical predictions of models of gas-rich mergers, seem to suggest that Arp 244 has the ultraluminous extreme starburst potential when merging proceeds into late stage. Arp 244 appears to be a snapshot of an ULIG in its early stage of making.

6. Multi-wavelength comparison together with numerical models appear to indicate that Arp 244 has recently passed the peak of large scale active star formation. Globally, the bulk of the molecular gas in Arp 244 is currently not in a starburst phase. The confined bona fide starburst sites of the highest SFE appear to be offsets from

the peaks of the CO, radio continuum, FIR, and MIR emission. The future ultraluminous extreme starburst phase can possibly be reached once the CO concentrations in the overlap merge with the double-nucleus gas concentrations in the final coalescence.

7. In conclusion, our newly determined 5.7 times larger total molecular gas mass in the “Antennae” galaxies lowers the global SFE to be comparable with that of GMCs in the Milky Way disk. Comparing the CO images with other observations, including our own VLA 20 cm continuum imaging, an overall relatively low molecular gas density and a low SFE across over the bulk of the molecular gas distribution have been revealed, which is in sharp contrast with most LIGs/ULIGs. The strongest starburst sites are currently confined in small regions heavily obscured in the dusty patches. We conclude that the large reservoir of molecular gas is the sufficient fuel for Arp 244 to ultimately enter an ultraluminous extreme starburst phase as merging proceeds to the advanced stage. The ultraluminous phase is possibly achieved once almost all molecular gas condenses into \sim kpc scale, with an order of magnitude increase in the gas surface density and more than ten-fold higher SFE.

We thank the NRAO 12m staff for generous supports and additional allocations of the observing time. We are grateful to the referee David Sanders and the Scientific Editor Gregory Bothun for helpful comments and suggestions. We also thank Robert Gruendl for assistance with some of the observations and helpful suggestions to an earlier version of this paper. Y.G. & K.Y.L. acknowledge support from the Laboratory of Astronomical Imaging which is funded by NSF grant AST 96-13999 and by the University of Illinois. K.Y.L., T.H.L., & S.W.L. acknowledge support from the Academia Sinica. Y.G. is also grateful to E.R. Seaquist for various support at the University of Toronto. This research has made use of the NASA/IPAC Extragalactic Database (NED) which is operated by the Jet Propulsion Laboratory, California Institute of Technology, under contract with the National Aeronautics and Space Administration. Y.G. is currently supported by the Jet Propulsion Laboratory, California Institute of Technology, under contract with NASA.

REFERENCES

- Aalto, S., Booth, R.S., Black, J.H., & Johansson, L.E.B. 1995, *A&A*, 300, 369
- Alton, P.B., Xilouris, E.M., Bianchi, S., Davies, J., & Kylafis, N. 2000, *A&A*, 356, 795
- Amram, P., et al. 1992, *A&A*, 266, 106
- Barnes, J.E. 1988, *ApJ*, 331, 699
- Barnes, J.E., & Hernquist, L. 1991, *ApJ*, 370, L65
- Barnes, J.E., & Hernquist, L. 1996, *ApJ*, 471, 115
- Barnes, J.E., & Hernquist, L. 1998, *ApJ*, 495, 187
- Bicay, M.D., Helou, G., & Condon, J.J. 1989 *ApJ*, 338, L53
- Braine, J., Lisenfeld, U., Duc, P.-A., & Leon, S. 2000, *Nature*, 403, 867
- Brouillet, N., Henkel, C., & Baudry, A. 1992, *A&A*, 262, L5
- Bryant, P.M., & Scoville, N.Z. 1999, *AJ*, 117, 2632
- Bushouse, H.A., Telesco, C.M., & Werner, M.W. 1998, *AJ*, 115, 938
- Carlberg, R. G. 1999, in *The Formation of Galactic Bulges*, ed. C.M. Carollo, H.C. Ferguson, & R.F.G. Wyse, (Cambridge: Cambridge University Press), 64 (astro-ph/9903373)
- Combes, F., et al. 1994, *A&A*, **281**, 725
- Condon, J.J. 1992, *ARA&A*, 30, 575
- Condon J.J., Helou, G., Sanders, D.B., & Soifer, B.T. 1990, *ApJS*, 73, 359
- Condon, J.J., Huang, Z.-P., Yin, Q.F., & Thuan, T.X. 1991, *ApJ*, 378, 65
- Downes, D., & Solomon, P.M. 1998, *ApJ*, 507, 615
- Evans, R., Harper, A., & Helou, G. 1997, in *Extragalactic Astronomy in the Infrared*, eds. G. A. Mamon, Trinh Xuan Thuan, & J. Tran Thanh Van. (Paris: Editions Frontieres), 143
- Evans, A.S., Surace, J.A., & Mazzarella, J.M. 2000, *ApJ*, 529, L85

- Fabbiano, G., Schweizer, F., & Mackie, G. 1997, *ApJ*, 478, 542
- Fabbiano, G. et al. 2000, Chandra X-ray Observatory press releases
- Fischer, J., et al. 1996, *A&A*, 315, L97
- Gao, Y. 1996, Ph.D. thesis, State Univ. of New York at Stony Brook
- Gao, Y., et al. 1997, in *Star Formation Near and Far*, eds. S.S. Holt, & L.G. Mundy (AIP: New York), 319
- Gao, Y., et al. 1999, in *Galaxy Interactions at Low and High Redshift*, IAU 186, ed. J.E. Barnes & D.B. Sanders (Dordrecht: Kluwer), 227
- Gao, Y., & Solomon, P.M. 1999, *ApJ*, 512, L99
- Gao, Y., & Solomon, P.M. 2000a, *ApJ*, submitted
- Gao, Y., & Solomon, P.M. 2000b, *ApJ*, submitted
- Gao, Y., & Xu, C. 2000, *ApJ*, 542, L83
- Genzel, R., Lutz, D., Sturm, E., et al. 1998, *ApJ*, 498, 579
- Haas, M., et al. 2000, *A&A*, 356, L83
- Helou, G., Soifer, B.T., & Rowan-Robinson, M. 1985, *ApJ*, 298, L7
- Helfer, T.T., & Blitz, L. 1997a, *ApJ*, 478, 162.
- Helfer, T.T., & Blitz, L. 1997b, *ApJ*, 478, 233.
- Hibbard, J.E., et al. 1994, *AJ*, 107, 67
- Hibbard, J.E., & van Gorkom, J.H. 1996, *AJ*, 111, 655
- Hibbard, J.E., & Yun, M.S. 1996, in *Cold Gas at High Redshift*, ed. M. N. Bremer, P. P. Van der Werf, H.J.A. Röttgering, & C.L. Carilli (Dordrecht: Kluwer), 47
- Hummel, E. & van der Hulst, J.M. 1986, *A&A*, 155, 151
- Hwang, C.-Y. et al. 1999, *ApJ*, 511, L17
- Jog, C.J., & Solomon, P.M. 1992, *ApJ*, 387, 152
- Kennicutt, R.C. 1998, *ApJ*, 498, 541
- Kunze, D., et al. 1996, *A&A*, 315, L101
- Lo, K.Y., Gao, Y., & Gruendl, R.A. 1997, *ApJ*, 475, L103
- Lo, K.Y., et al. 2000, in *Galaxy Dynamics: from the Early Universe to the Present*, ed. F. Combes, G. A. Mamon, & V. Charmandaris, ASP Conf. Ser., 112, 279
- Lu, N.Y., et al. 1996, *A&A*, 315, L153
- Marsh, K.A., & Helou, G. 1995, *ApJ*, 445, 599
- Mihos, J.C., & Hernquist, L. 1996, *ApJ*, 464, 641
- Mihos, J.C., Bothun, G.D., & Richstone, D.O. 1993, *ApJ*, 418, 82
- Mirabel, I.F., & Sanders, D.B. 1988, *ApJ* 335, 104
- Mirabel, I.F., & Sanders, D.B. 1989, *ApJ* 340, L53
- Mirabel, I.F., Dottori, H., & Lutz, D. 1992, *A&A*, 256, L19
- Mirabel, I.F., et al. 1998, *A&A*, 333, L1
- Murphy, T.W. 2000, Ph.D. thesis, California Institute of Technology
- Neff, S. G., & Ulvestad, J. S. 2000, *AJ*, 120, 670
- Nikola, T., et al. 1998, *ApJ*, 504, 749
- Noguchi, M. 1991, *MNRAS*, 251, 360
- Olson, K.M., & Kwan, J. 1990, *ApJ*, 349, 480
- Olson, K.M., & Kwan, J. 1990, *ApJ*, 361, 426
- Read, A. M., Ponman, T. J., & Wolstencroft, R. D. 1995, *MNRAS*, 277, 397
- Rubin, V.C., Ford, W.K., & D'Odorico, S. 1970, *ApJ*, 160, 801
- Sakamoto, K., et al. 1999, *ApJ*, 514, 68
- Mirabel 1985 Sanders, D.B., & Mirabel, I.F. 1985, *ApJ*, 298, L31
- Sanders, D.B., et al. 1988, *ApJ*, 325, 74.
- Sanders, D.B., & Mirabel, I.F. 1996, *ARA&A*, 34, 749
- Sanders, D.B. 1999, *Ap&SS*, 266, 331 (astro-ph/9908297)

- Schweizer, F. 1978, in IAU Symp. 77, Structure and Properties of Nearby Galaxies, ed. E.M. Berkhuijsen & R. Wielebinski (Dordrecht: Reidel), 279
- Scoville, N. Z., Sargent, A. I., Sanders, D. B., & Soifer, B. T. 1991, ApJ, 366, L5
- Scoville, N.Z., Yun, M.S., & Bryant, P. M. 1997, ApJ, 484, 702
- Scoville, N.Z., et al. 2000, AJ, 119, 991
- Smith, B. J. & Higdon, J. L. 1994, AJ, 108, 837
- Smith, H.E., Lonsdale, C.J., & Lonsdale, C.J. 1998, ApJ, 492, 137
- Soifer, B.T., et al. 1989, AJ, 98, 766
- Soifer, B.T., et al. 2000, AJ, 119, 509
- Solomon, P.M., Downes, D., & Radford, S.J.E. 1992, ApJ, 387, L55
- Solomon, P.M., et al. 1997, ApJ, 478, 144
- Solomon, P.M., & Barrett, J.W. 1991, in IAU Symp. 146, Dynamics of Galaxies and Their Molecular Cloud Distributions, ed. F. Combes & F. Casoli, (Dordrecht: Kluwer), 235
- Stacey, G.J., et al. 1991, ApJ, 373, 423
- Stanford, S.A., Sargent, A.I., Sanders, D.B., & Scoville, N.Z. 1990, ApJ, 349, 492
- Surace, J.R., Sanders, D.B., Vaca, W.D., & Veilleux, S. 1998, ApJ, 492, 116
- Tacconi, L.J., et al. 1999, ApJ, 524, 732
- Toomre, A., & Toomre, J. 1972, ApJ, 178, 623
- Toomre, A. 1977, in The Evolution of Galaxies and Stellar Populations, ed. B.M. Tinsley B.M., & R.B. Larson (New Haven: Yale Univ.), 401
- van der Hulst, J.M. 1979, A&A, 71, 131
- Veilleux, S., Sanders, D.B., & Kim, D.C. 1999, ApJ, 522, 139
- Vigroux, L., et al. 1996, A&A, 315, L93
- Walter, F., & Heithausen, A. 1999, ApJ, 519, L69
- Wang, W.-H., Lo, K.Y., Gao, Y., & Gruendl, R.A. 2000, AJ, submitted
- Whitmore, B.C., Zhang, Q., Leitherer, C., Fall, S.M., Schweizer, F., & Miller, B.W. 1999, AJ, 118, 1551
- Wilson, C.D., Scoville, N.Z., Madden, S.C., & Charmandaris, V. 2000, ApJ, in press
- Xu, C., et al. 1994, A&A, 282, 19
- Xu, C., Gao, Y., Mazzarella, J., et al. 2000, ApJ, 541, 644
- Young, J.S., et al. 1995, ApJS, 98, 219
- Young, J.S., & Scoville, N. Z. 1991, ARA&A, 29, 581

This 2-column preprint was prepared with the AAS L^AT_EX macros v5.0.

TABLE 1
SUMMARY OF THE NRAO 12M CO MAPPING RESULTS

No.	R.A. ^a arcsec	Decl. ^a arcsec	I_{CO}^{b} K km s ⁻¹	V_{CO} km s ⁻¹	ΔV_{FWHM} km s ⁻¹
1	0.0	0.0	19.5	1632	93
2	0.0	27.5	11.9	1612	204
3	0.0	-27.5	20.1	1607	201
4	0.0	55.0	5.2	1607	282
5	0.0	82.5	3.5	1561	331
6	0.0	-82.5	10.6	1659	281
7	0.0	-55.0	19.2	1604	227
8	0.0	110.0	0.4 ^c	1663	110
9	0.0	-110.0	3.9	1638	348
10	0.0	-137.5	1.3	1660	229
11	27.0	0.0	21.5	1593	198
12	27.0	27.5	13.6	1610	280
13	27.0	-27.5	26.9	1565	200
14	27.0	55.0	3.4	1567	229
15	27.0	-55.0	27.4	1567	245
16	27.0	82.5	2.5	1553	289
17	27.0	-82.5	14.0	1604	270
18	27.0	110.0	... ^d
19	27.0	-110.0	2.6	1698	166
20	27.0	-137.5	1.2 ^c	1618	308
21	-27.0	0.0	14.4	1627	165
22	-27.0	27.5	9.6	1609	144
23	-27.0	-27.5	13.0	1598	255
24	-27.0	55.0	4.4	1582	150
25	-27.0	-55.0	7.7	1621	279
26	-27.0	82.5	2.7	1626	241
27	-27.0	-82.5	5.3	1658	321
28	-27.0	110.0	2.2	1568	463
29	-27.0	-110.0	3.7	1640	302
30	-27.0	-137.5	... ^d
31	53.9	0.0	11.8	1592	213
32	53.9	27.5	7.7	1572	246
33	53.9	-27.5	18.9	1558	215
34	53.9	55.0	2.4	1648	204
35	53.9	-55.0	19.8	1560	193
36	53.9	82.5	1.2	1652	241
37	53.9	-82.5	9.1	1597	254
38	53.9	-110.0	2.7	1630	360
39	53.9	-137.5	1.5	1651	283
40	-53.9	0.0	9.4	1628	241
41	-53.9	27.5	3.3	1622	222

TABLE 1—*Continued*

No.	R.A. ^a arcsec	Decl. ^a arcsec	I_{CO}^{b} K km s ⁻¹	V_{CO} km s ⁻¹	ΔV_{FWHM} km s ⁻¹
42	-53.9	-27.5	4.4	1669	245
43	-53.9	55.0	2.2	1616	388
44	-53.9	-55.0	2.3	1696	62
45	-53.9	82.5	1.1 ^c	1547	150
46	-53.9	-82.5	0.9 ^c	1788	25
47	-53.9	-110.0	2.2	1598	323
48	80.9	0.0	4.5	1607	316
49	80.9	27.5	2.3	1567	235
50	80.9	-27.5	6.5	1567	228
51	80.9	55.0	0.6 ^c	1734	147
52	80.9	-137.5	1.2 ^c	1725	127
53	-80.9	0.0	1.7	1642	53
54	-80.9	27.5	2.4	1650	303
55	-80.9	-27.5	1.6	1632	242
56	-80.9	55.0	0.6 ^c	1600	157
57	-80.9	-55.0	0.4 ^c	1638	21
58	-80.9	-82.5	0.5 ^d	1571	74
59	109.3	0.0	1.2	1554	186
60	109.3	27.5	1.3 ^c	1697	152
61	109.3	-27.5	0.9 ^c	1610	179
62	-107.9	0.0	... ^d
63	-107.9	27.5	1.0 ^c	1502	100
64	-107.9	-27.5	0.4 ^c	1599	54
65 ^e	81.8	-55.0	4.6	1538	213
66 ^e	109.3	-82.5	1.7	1584	178
67 ^e	81.8	-82.5	3.5	1575	284
68 ^e	81.8	-110.0	0.9	1629	251
69 ^e	109.3	-55.0	1.7	1564	201
70 ^e	109.3	-110.0	1.7	1617	324
71 ^e	136.8	-55.0	0.4 ^c	1588	30
72 ^e	136.8	-82.5	1.2 ^c	1644	370
73 ^e	136.8	-110.0	0.5 ^d	1520	300
74	25.9	-39.1	34.3	1558	209

^aOffsets relative to RA=12^h01^m53.1^s, Dec=-18°52′05.″0 (J2000, the nucleus of NGC 4038).

^bIntegrated CO line intensity, which is calculated using the same broad line emission window of 1300 to 1900 km s⁻¹. The Jy/K (T_{R}^*) conversion adopted is ~ 35 Jy/K. Some offsets have slightly larger I_{CO} when a narrower line emission window is used.

^cTentative detections ($\gtrsim 3\sigma$).

^dNon-detections ($< 3\sigma$).

^eDeep CO spectra are shown in Figure 5a.

TABLE 2
GLOBAL PROPERTIES OF ARP 244

Parameter	Value	References
d_L	20 Mpc	van der Hulst 1979; Mirabel et al. 1998
L_B	$2.9 \times 10^{10} L_\odot$	from B mag. in RC3
L_{IR}	$6.2 \times 10^{10} L_\odot$ (<i>IRAS</i>)	Soifer et al. 1989; Sanders et al. 2001 in prep.
L_{IR}	$8.0 \times 10^{10} L_\odot$ (KAO)	Bushouse et al. 1998
I_{CO}	90.6 K km s^{-1} (T_R^*)	this work
$S_{CO} dV$	$3172 \text{ Jy km s}^{-1}$	this work
L_{CO}	$0.3 \times 10^{10} \text{ K km s}^{-1} \text{ pc}^2$ (T_{mb})	this work
$M(\text{H}_2)$	$1.5 \times 10^{10} M_\odot$	this work
$L_{IR}/M(\text{H}_2)$	$4.2 L_\odot/M_\odot$	this work
$M(\text{HI})$	$0.4 \times 10^{10} M_\odot$	van der Hulst 1979; Hibbard et al. 2001 in prep.
M_{dust}	$\sim 10^8 M_\odot$	Haas et al. 2000
$M_{\text{gas}}/M_{\text{dust}}$	~ 190	this work
L_{HCN}	$0.7 \times 10^8 \text{ K km s}^{-1} \text{ pc}^2$ (T_{mb})	this work
L_{HCN}/L_{CO}	0.02	this work
$M(\text{H}_2)_{\text{tidal dwarf}}$	$\gtrsim 2 \times 10^8 M_\odot$	this work

0010128.fig1.gif

Fig. 1. DSS image of Arp 244 (the “Antennae” galaxies) and the locations of our deep HCN and CO search. Thin circles are CO beams, observed at southeastern edge of the disk overlap where the southern tidal tail begins, and at the tidal dwarf galaxy near the tip of the southern tail. The thick circles mark the two HCN beams. The southern HCN beam covers both the overlap and the nuclear region of NGC 4039.

0010128.fig2.gif

Fig. 2. Fully mapped NRAO 12m CO(1-0) integrated intensity map (in contours) overlaid on the HST/WFPC2 image. The contours are 3, 4, 6 to 28 K km s^{-1} (in increases of 2 K km s^{-1} on a T_R^* scale). The CO spectra at each of the observed position are also plotted (velocity ranges from 1150 to 2050 km s^{-1} , and T_R^* ranges from -25 to 155 mK). The currently accepted total molecular gas mass in the literature was based upon only one beam measurement near the CO peak position (Sanders & Mirabel 1985). Obviously one NRAO 12m beam (top left) does not capture anywhere even near the CO emission from the overlap region. We have sampled 73 positions at half-beam spacing to ensure that no further extended CO emission was significantly detected in the outer edge, in typically 1.5 hr of the integration time.

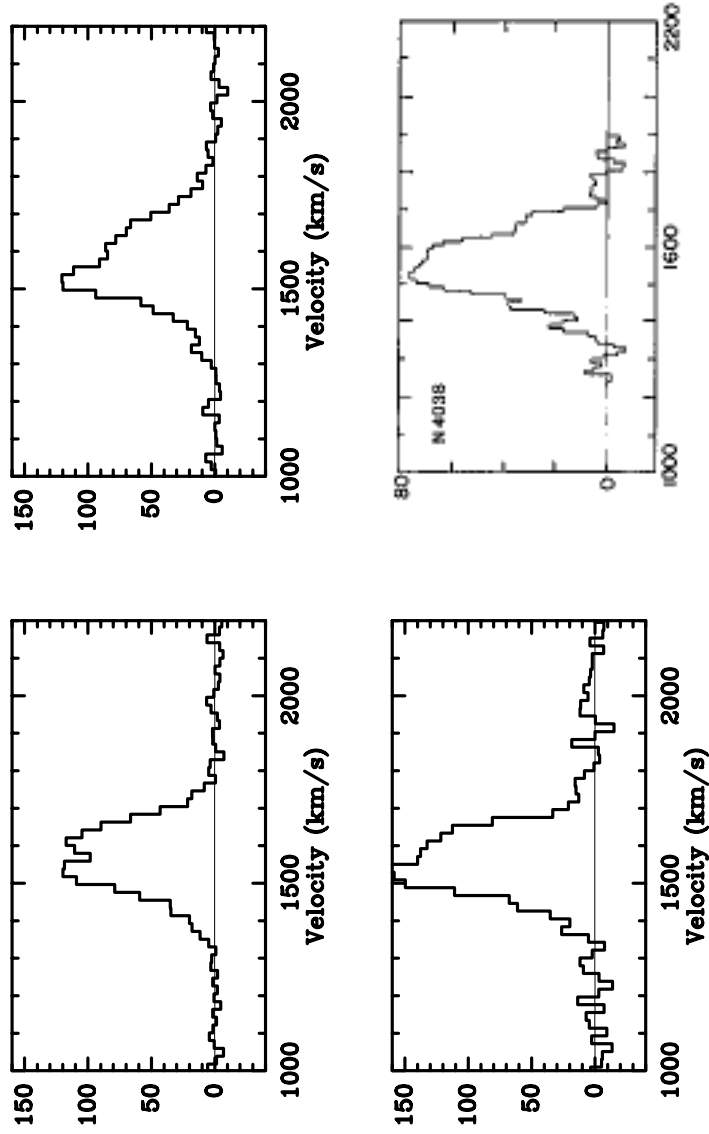


Fig. 3.

CO spectra closest to the peak CO emission in the overlap region compared with the old CO spectrum of Sanders & Mirabel (1985). We detected broader CO profile, which was previously missed due to insufficient velocity coverage in the old CO observation, and stronger CO emission.

0010128.fig4a—4e.gif

Fig. 4a—4e. CO integrated intensity maps (contours) in 100 km s^{-1} velocity width. All contours plotted are $0.4, 0.7$ to 2.5 K km s^{-1} in increases of 0.3 K km s^{-1} .

0010128.fig4f.gif

Fig. 4f. The CO integrated intensity map over the total velocity range (essentially same as the contour map in Figure 2, but here all CO data have been used), which has contours 1.4, 2, 3, 4, 6 to 34 K km s^{-1} , in increases of 2 K km s^{-1} .

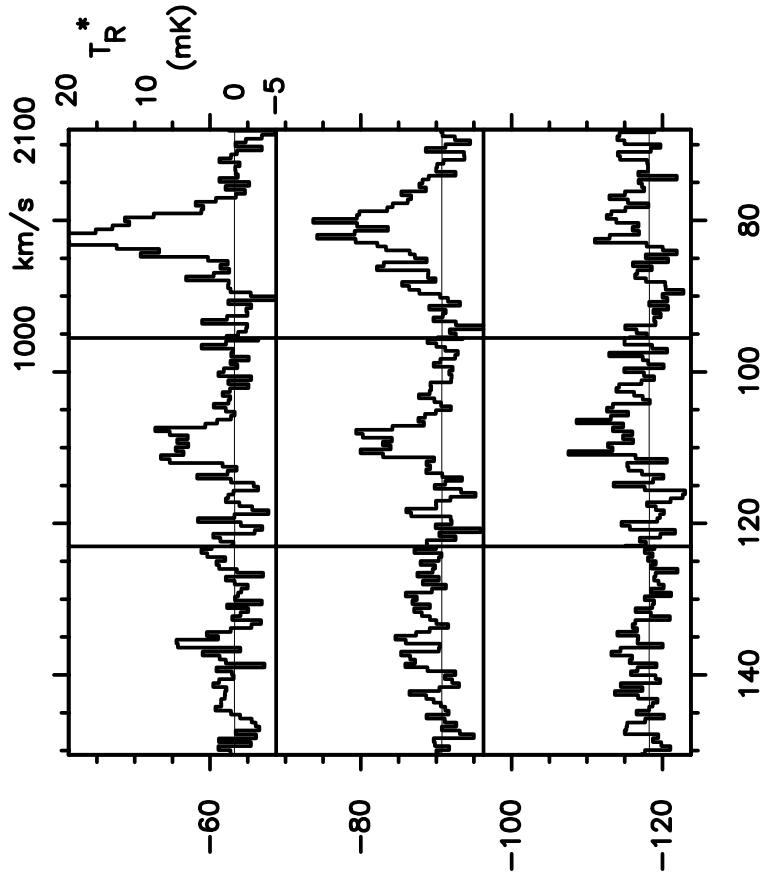


Fig. 5a. The deep CO(1-0) spectra near the southeastern (SE) edge of the overlap region (the SE corner of the merging disks in Fig. 1). The numbers refer to the offsets in arcsec, with respect to the northern nucleus, and the central position here corresponds to an offset of $(110'', -82.5'')$. Fig. 5b. Both the summed average spectrum (top) from all 5 positions searched for CO (more than 27 hours integration) in the tidal dwarf galaxy, and the deep integration spectrum (bottom) at position of RA=12:01:26.0, DEC=-19:00:37.5 (J2000) (more than 12 hour integration), show tentative weak detections. Fig. 5c. HCN(1-0) spectra obtained from the northern galaxy NGC 4038 and from the overlap region plus the southern galaxy NGC 4039.

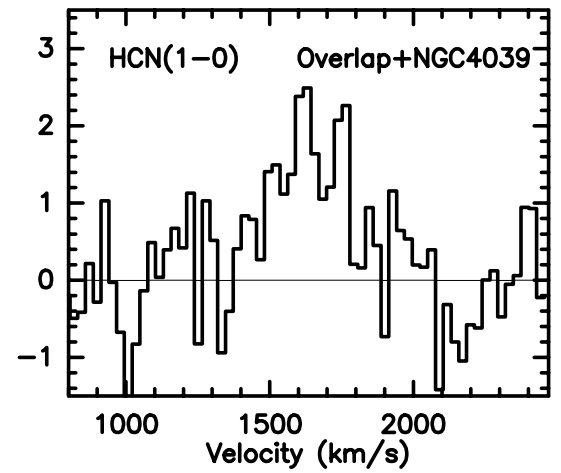
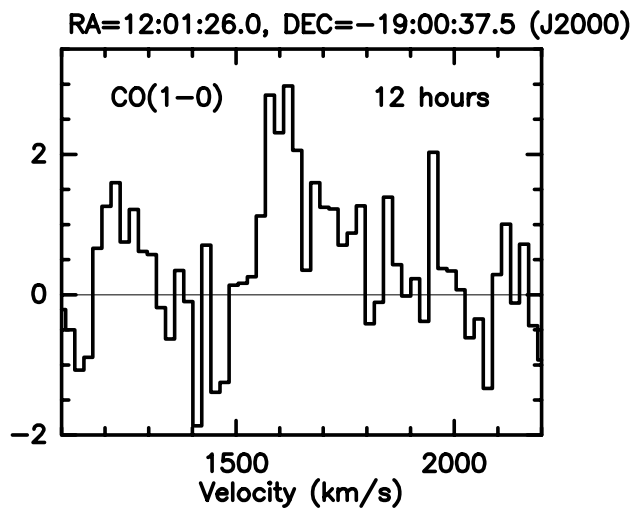
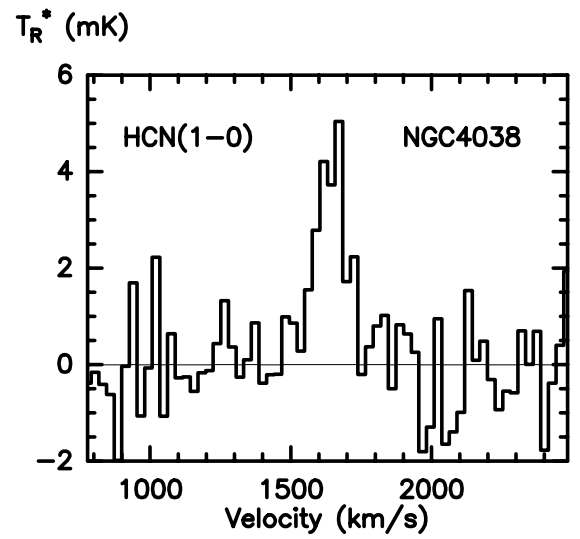
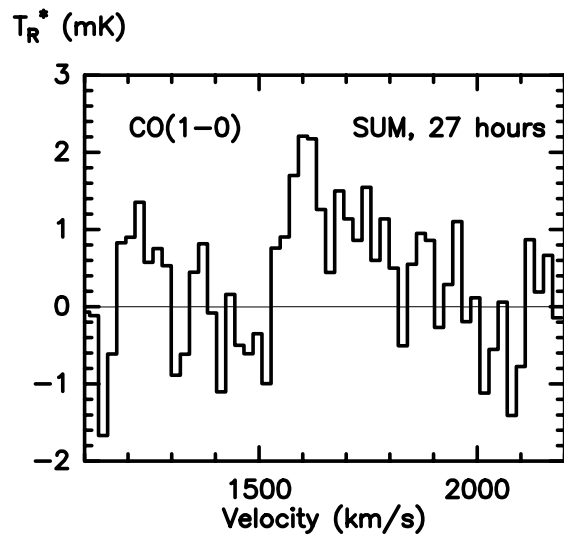


Fig. 5b.

Fig. 5c

0010128.fig6.gif

Fig. 6. The 20cm radio continuum to CO(1-0) emission ratio map (contours) compared with the HST/WFPC2 image (gray-scale). This illustrates the sites of the most intense starbursts of the highest star formation efficiency (SFE). White contours indicate the sites of the highest ratios, ~ 5 times above the average, suggesting the highest SFE $\gtrsim 20 L_{\odot}/M_{\odot}$. Black contours are the sites of a factor of 2 lower in the radio-to-CO ratios, implying a SFE $\gtrsim 10 L_{\odot}/M_{\odot}$.

0010128.fig7.gif

Fig. 7. The overall ratio map (contours) of the 20cm radio continuum to the CO emission compared with the VLA 20cm radio continuum image (gray-scale). Here black contours are the sites of the highest radio-to-CO ratios (same as those white contours in Figure 6) and the ones a factor of 1.5 lower, gray contours are for the radio-to-CO ratios of a factor of 2 lower than the highest (same as those black contours in Figure 6) and those a factor of 1.5 further lower, and white contours here are for the lowest radio-to-CO ratios, a factor of 4 and 6 lower than the highest, indicating the sites of $SFE \sim 5L_{\odot}/M_{\odot}$ and lower, about the average SFE across over the entire system.

This figure "fig1.gif" is available in "gif" format from:

<http://arxiv.org/ps/astro-ph/0010128v2>

This figure "fig2.gif" is available in "gif" format from:

<http://arxiv.org/ps/astro-ph/0010128v2>

This figure "fig4a.gif" is available in "gif" format from:

<http://arxiv.org/ps/astro-ph/0010128v2>

This figure "fig4b.gif" is available in "gif" format from:

<http://arxiv.org/ps/astro-ph/0010128v2>

This figure "fig4c.gif" is available in "gif" format from:

<http://arxiv.org/ps/astro-ph/0010128v2>

This figure "fig4d.gif" is available in "gif" format from:

<http://arxiv.org/ps/astro-ph/0010128v2>

This figure "fig4e.gif" is available in "gif" format from:

<http://arxiv.org/ps/astro-ph/0010128v2>

This figure "fig4f.gif" is available in "gif" format from:

<http://arxiv.org/ps/astro-ph/0010128v2>

This figure "fig6.gif" is available in "gif" format from:

<http://arxiv.org/ps/astro-ph/0010128v2>

This figure "fig7.gif" is available in "gif" format from:

<http://arxiv.org/ps/astro-ph/0010128v2>